Environmental Science & Technology

Article

pubs.acs.org/est

Does Hindered Transport Theory Apply to Desalination Membranes?

Emil Dražević,[†] Krešimir Košutić,[†] Vesselin Kolev,[‡] and Viatcheslav Freger*[,‡]

[†]Faculty of Chemical Engineering and Technology, University of Zagreb, Marulićev trg 19, 10000 Zagreb, Croatia

[‡]Wolfson Department of Chemical Engineering, Technion - Israel Institute of Technology, Technion City, 32000 Haifa, Israel

Supporting Information

ABSTRACT: As reverse osmosis (RO) and nanofiltration polyamide membranes become increasingly used for water purification, prediction of pollutant transport is required for membrane development and process engineering. Many popular models use hindered transport theory (HTT), which considers a spherical solute moving through an array of fluid-filled rigid cylindrical pores. Experiments and molecular dynamic simulations, however, reveal that polyamide membranes have a distinctly different structure of a "molecular sponge", a network of randomly connected voids widely distributed in size. In view of this disagreement, this study critically examined the validity of HTT by directly measuring diffusivities of several alcohols within a polyamide film of commercial RO membrane using attenuated total reflection−FTIR. It is found that measured diffusivities deviate from HTT predictions by as much as 2−3 orders of magnitude. This result indicates that HTT does not adequately describe solute transport in desalination membranes. As a more adequate alternative, the concept of random resistor networks is suggested, with resistances described by models of activated transport in "soft" polymers without a sharp size cutoff and with a proper address of solute partitioning.

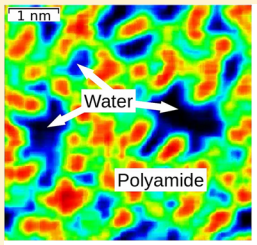

MD: sponge-like structure

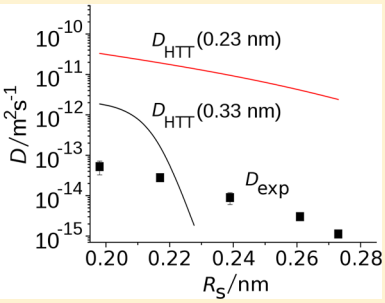

INTRODUCTION

Reverse osmosis (RO) and nanofiltration (NF) are commonly used to remove inorganic and organic pollutants from water and have become an integral part of the environmental technology toolbox.[1,2] Unfortunately, these processes have limitations and, as the rejections of many organics are often reasonably high,[3] some organic pollutants pass the membranes to a significant degree. The removal mechanism for organics is still poorly understood and predictive modeling presents a significant challenge.[4]

Most models proposed so far employ the hindered transport theory (HTT) assuming that membrane acts as an array of cylindrical pores through which the solute passes.[2] The theory dates back to the work of Ferry[5] in 1936; most notable other contributions are those by Brenner and collaborators.[6−8] Deen summarized five decades of research in a comprehensive review.[9] The transport in HTT is modeled by considering the hydrodynamic interactions experienced by a spherical solute moving in a pore filled with a uniformly viscous bulk-like continuum. If necessary, the model may also incorporate a partitioning effect due to interactions with the surrounding matrix, e.g., with the fixed charges at the pore surface in the case of charged solutes. The key parameter in HTT relations is the ratio of solute and pore radii that ultimately determines hindrance corrections to diffusion (K_d) and convection (K_c) relative to the unhindered transport in the bulk. HTT has been experimentally verified in cylindrical pores down to pore sizes of 3 nm, with good agreement between the experiment and theoretical predictions.[9]

Although the theory was originally devised for microparticles and macromolecules in micropores, it has been extended to subnano (molecular) pores and solutes and applied to RO[3,9,10] and NF[11,12] for predicting hindrance of molecules within the swollen active layer.[1,13−15] Verliefde et al. pointed out that agreement could be significantly improved by addressing partitioning of organic solutes.[1]

Estimates of solute hindrance critically depend on the pore radius. In the polyamide RO and NF membranes they typically range from 0.2 to 0.5 nm.[16,17] Many such estimates are based on hydraulic permeability or rejection of probe solutes, analyzed essentially using HTT itself, again, assuming the pores are parallel and cylindrical. An alternative technique for measuring the pore size is positron annihilation lifetime spectroscopy study (PALS), producing fairly similar results.[16] However, recent molecular dynamic studies of cross-linked aromatic polyamide RO membranes reveal a far more complex sponge-like structure containing nanovoids widely distributed in size.[18−22] Voids are highly irregular and separated by fragments of a dense polymer or narrow passages that often have a slit-like rather than cylindrical geometry, as the aromatic polyamides tend to form near-planar structures packed into stacks.[22] Interpretation of PALS data usually assumes the pores are spherical, which may approximate the shape of the voids,

Received: April 29, 2014
Revised: August 2, 2014
Accepted: August 19, 2014

   dx.doi.org/10.1021/es502085p | Environ. Sci. Technol. XXXX, XXX, XXX−XXX

but not necessarily the passages connecting the voids. Interpretation of the pore size based on the above data is therefore not straightforward. It may be further complicated by nonideal shape of the pores and solutes, deviation of water viscosity from its bulk value through disruption of the hydrogen bonds,[18−22] existence of additional nonhydrodynamic kinetic barriers, and, in general, inapplicability of the macroscopic hydrodynamic approach at molecular scales. Given the popularity of HTT in today's models of NF and RO and their importance in environmental technologies, it is of significant interest to understand the limitations and critically examine the validity of the HTT in these processes.

Surprisingly, the applicability of HTT has not been directly tested for RO and NF. We propose here to examine for this purpose the solute diffusivity that is directly measurable by certain techniques. Diffusivities of some solutes in aromatic polyamide have been measured by several methods. Frommer et al.[23] measured diffusivity of NaCl in aromatic polyamide by NMR and obtained values of an order of 10^{-14} m^2 s^{-1}, in line with estimates by Bason et al. using impedance spectroscopy.[24] Dražević et al. reported similarly low values for the small organic solutes hydroquinone and benzoquinone.[4] This is far lower than HTT estimates for small molecules in 0.2−0.5 nm pores, which are rarely below 10^{-12} m^2 s^{-1}, suggesting that HTT could significantly overestimate diffusion coefficients in RO/NF.

In this study, a simple nondestructive method of Fieldson and Barbari[25] is used for measuring diffusion coefficients in thin polymer films exposed to solution.[26] In this technique the intensity of a solute band is monitored over time using attenuated total reflection Fourier-transform infrared (ATR−FTIR) spectroscopy in a setup schematically shown in Figure 1.

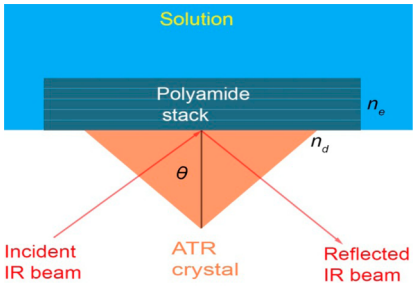

Figure 1. ATR−FTIR diffusion setup: ATR crystal with a stack of polyamide films on top exposed to a solution.

The diffusivity of *n*-alcohols of different sizes in the polyamide layer of a seawater membrane SWC4+ is found by fitting to a model based on the diffusion kinetics and laws of ATR optics.[25] Such results could be directly compared to HTT predictions.

THEORETICAL BACKGROUND

Analysis of Solute Diffusion in a Polymer Film by ATR−FTIR. For a setup, schematically shown in Figure 1, for a given film thickness, the variation of the intensity of a band associated with the solute after a step-like increase of the solute concentration in solution at $t = 0$ is given by the following expression:[22,23]

$$\frac{A(t) - A(0)}{A(\infty) - A(0)} = 1 - \frac{8\gamma}{\pi[1 - \exp(-2\gamma d_{wet})]} \sum_{N=0}^{\infty} \frac{\exp(g)[f\exp(-2\gamma d_{wet}) + (-1)^N(2\gamma)]}{(2N+1)(4\gamma^2 + f^2)} \quad (1)$$

where $g = D(2N+1)^2\pi^2 t/4d_{wet}^2$ and $f = (2N+1)\pi/d_{wet}$.

In eq 1, $A(t)$ is the intensity at time t, $A(\infty)$ is the maximum intensity at infinite t, i.e., in equilibrium with solution, d_{wet} is the thickness of the swollen (wet) film, D is the average diffusivity of the solute in the film in the normal direction, and γ is the reciprocal penetration depth of the specific band in the film, given by the following formula:

$$\gamma = \frac{2\pi\sqrt{n_e^2 \sin^2\theta - n_d^2}}{\lambda} \quad (2)$$

In eq 2 n_e is the effective refractive index of the film, $\theta = \pi/4$ is the angle of incidence of the IR beam at the film-crystal interface, n_d is the refractive index of the ATR crystal, and λ is the wavelength of the band. The value of n_e in eq 2 was calculated using the Bruggeman formula based on the effective medium approximation.[27]

$$\Phi\frac{n_w - n_e}{n_w + 2n_e} + (1 - \Phi)\frac{n_p - n_e}{n_p + 2n_e} = 0 \quad (3)$$

where $n_w = 1.33$ and $n_p = 1.65$ are the refractive indices of water and aromatic polyamide, respectively, and Φ is the water content in the film, which was measured by AFM in this study, as described in the Experimental Section. The two unknowns in eq 1, D and $A(\infty)$, are estimated by fitting the model to the experimental data using $N = 1000$ terms.

Hindered Transport Theory (HTT) Relations. Bulk diffusion coefficients of organics used in this study along with their corresponding Stokes radii are presented in the Supporting Information (SI) Table S1. To be consistent with eq 1 the diffusion coefficient D of a particular organic solute in the membrane is related to hindrance and tortuosity as follows:[9]

$$D = \frac{K_d(\varphi)}{\alpha} D_\infty \quad (4)$$

Here D_∞ is the bulk diffusion coefficient of the solute (SI Table S1), $K_d(\varphi)$ is the diffusive hindrance factor, depending on the ratio of the solute radius to pore radius, $\varphi = R_s/R_p$, and α is the tortuosity factor. The solute radius R_s is usually identified with the Stokes radius deduced from D_∞. Note that HTT relations used for modeling membrane transport usually consider transport *within the pores* normalized to "external" concentration difference between up- and downstream solutions thereby they contain a partitioning factor. In contrast, eq 4 refers to the concentration gradient defined "internally", i.e., in the same phase, in which diffusion takes place. This definition reflects the situation encountered in ATR−FTIR measurements, where the band intensity corresponds to the laterally averaged concentration *within* the film. Equation 4 then gives the average solute diffusivity in the normal direction and should include no partitioning factor, neither steric nor molecular interaction-related, totally decoupling the diffusion from partitioning and allowing a direct test of hindrance relations. Equation 4 also allows the parallel cylindrical pores to become tortuous, thus the tortuosity factor α accounts for increased

dx.doi.org/10.1021/es502085p | Environ. Sci. Technol. XXXX, XXX, XXX−XXX

pore length and for decreased concentration gradient along this path.

Bungay and Brenner[7] developed the following HTT correlation for computing the function $K_d(\varphi)$ based on the center-line approximation[9] valid for the entire range $0 < \varphi < 1$:

$$K_d = \frac{6\pi}{K_t}, \text{ and } K_t = \frac{9}{4}\pi^2\sqrt{2}(1-\varphi)^{-5/2}\left(1 + \sum_{n=1}^{2} a_n(1-\varphi)^n\right) + \sum_{n=0}^{4} a_{n+3}\varphi^n \quad (5)$$

where $a_1 = -1.2167$, $a_2 = 1.5336$, $a_3 = -22.5083$, $a_4 = -5.6117$, $a_5 = -0.3363$, $a_6 = -1.216$, and $a_7 = 1.647$. The dependence given by eq 5 is shown in SI Figure S1. Improved or simpler correlations are often used for more restricted ranges of φ,[8,12] they insignificantly differ from eq 5 thereby the latter was preferred here as one that covers the full range of φ. The tortuosity factor α in general depends on the total fraction and microstructure of the pores. However, under the assumption of sufficient randomness of the pores, dependence of α on porosity (i.e., water fraction) becomes fairly insensitive to microstructural details (see next section).

Evaluation of the Effective Pore Radii. An independent estimate of the effective pore radius R_p is crucial for HTT calculations. In this work two estimates of R_p were obtained by two different approaches: (a) a generalized Kozeny−Carman relation[28,29] connecting R_p to the pure water permeability and porosity (water fraction), and (b) surface force−pore flow (SFPF) model relating R_p to rejection of an independent set of model solutes.[30] Similar to eq 4, the former relation views the medium as a network of tortuous cylindrical pores, as follows:

$$R_p = \sqrt{\frac{L_p d_{wet}\eta\alpha}{b\Phi}} \quad (6)$$

Equation 6, is a generalization of the classical Kozeny−Carman equation, where L_p is the pure water permeability, η is the viscosity of the water in the pores (identified with the bulk viscosity), d_{wet} is the measured swollen thickness of the membrane, Φ is the water fraction (identified with porosity), and α is the tortuosity factor. Tortuosity may be estimated using its dependence on porosity (water content), numerically estimated by Torquato[31] and employed by Bason et al.[29] Torquato[31] suggests using $b = 1/8$ for random porous media, as assumed here for the polyamide layer of SWC4+.

The second approach employs the SFPF model, originally developed by Sourirajan and Matsuura.[32] This model is a simplified version of HTT; it views the membrane as an array of parallel pores with a pore size distribution and considers pore flow of solvent, steric partitioning, and convective hindrance, but neglects solute diffusion. In its original form the SFPF incorporates semiempirical corrections for solute interactions with the matrix and effects of finite size of the solvent, which were neglected here. The numerical procedure seeks the pore size distribution which fits both experimentally obtained water permeability and rejections of six ether solutes of different sizes.

EXPERIMENTAL SECTION

Preparation of the Polyamide Stacks for the AFM and FTIR Measurements. Sea water RO membrane SWC4+ (Hydranautics/Nitto Denko, Oceanside, CA, USA) was used in this study as representative of a dense RO membrane. It comprises three layers: an about 100 nm thick dense aromatic polyamide (PA) selective layer, a microporous polysulphone (PSU) support, and a polyester backing. The PSU/PA layer was peeled off the polyester layer, placed with the PA side facing the surface on a silicon wafer or ATR diamond crystal, and wetted with a drop of toluene. The latter softens both PA and PSU and leaves PSU/PA adhered to the surface by capillary forces after toluene evaporation. Thereafter, PSU was carefully dissolved away using dimethylformamide (DMF) and the film was dried of DMF in cold air flow from a hair dryer. Given that the thickness of SWC4+ membrane is about 100 nm,[28] and the penetration depth of the infrared beam is between 1−2 μm, the procedure was repeated $p \leq 10$ times to obtain a stack of p layers of a thickness commensurate with the penetration depth. Thickness and swelling of the stacks were measured using AFM, as proposed by Freger.[14]

Film Thickness and Water Content: AFM Measurements. The procedure for measuring the thickness of the dry and wet stacks of PA films are described in detail elsewhere.[28] Briefly, a stack on a Si wafer was gently scratched with a sharp needle and the thickness of the formed strips was measured at room temperature using a Bruker Innova AFM microscope. Bruker SNL cantilevers (triangular D), with the nominal spring constant 0.06 N/m, were used in contact mode and mounted on an APMC-0001 Microcell for liquid imaging. The samples were first imaged dry and then covered with DI water and the same location was rescanned in the wet state. The water content of one layer or the stack of layers was calculated using the following expression:

$$\Phi = (d_{wet} - d_{dry})/d_{wet} \quad (7)$$

In eq 7, d is the thickness, dry or wet, of one layer or stack of layers, as measured by AFM.

FTIR Diffusion Measurements Procedure. The organic solutes were 6 different alcohols: ethylene glycol, glycerol, 1-butanol, 1-pentanol, and benzyl alcohol. The choice of solutes was dictated by a minimal overlap with polyamide bands and a substantial partitioning, which facilitated monitoring of the OH band of alcohols around 1000 cm^{-1}.

The infrared spectra of PA films were recorded at a rate 1.64 s per spectrum at resolution 2 cm^{-1} in the mid-IR range (400−4000 cm^{-1}) using a Bruker Vertex 70 series FTIR spectrometer equipped with a Bruker Platinum ATR accessory with a single reflection diamond crystal ($n_d = 2.4$). Stacks of the SWC4+ films were isolated and attached directly to the crystal (Figure 1). A stainless steel liquid cell was mounted on top of the crystal to enclose the PA film, and diffusion measurements were performed using the following procedure. (1) Deionized (DI) water was injected into the liquid cell using a stainless steel syringe. (2) A sequence of spectra was recorded until no change was observed to verify the polyamide film (a single layer or a stack) equilibrated with water; 60 s after water injection was usually sufficient to reach equilibrium. (3) After equilibration with water, the spectrum of PA film in water was recorded as the background for subsequently recorded spectra. (4) A solution containing 0.2 M solution of a particular organic solute was injected and a sequence of spectra over time was recorded to monitor the change of the appropriate solute band.

All measurements were repeated three times for each solute, with each time using a new freshly prepared stack.

Reverse Osmosis Experiments. The RO cell with a feed spacer and the experimental procedure used are described in

dx.doi.org/10.1021/es502085p | Environ. Sci. Technol. XXXX, XXX, XXX−XXX

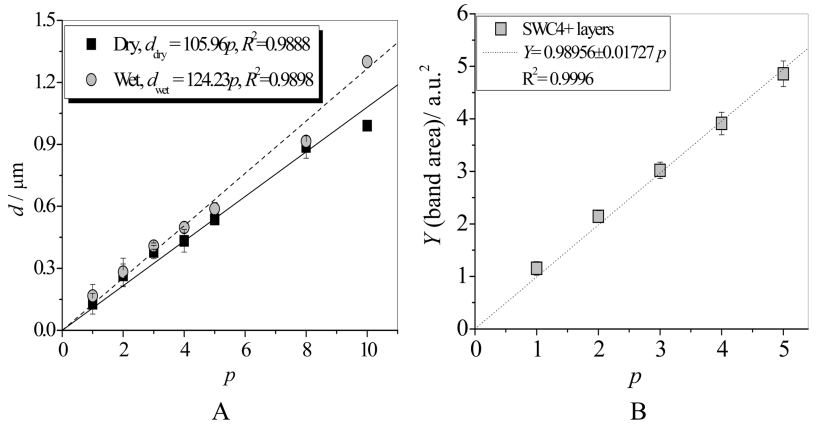

Figure 2. AFM and ATR−FTIR measurements on the stacks of layers. (A) Thickness of the stack, d, versus the number of layers, p, from AFM measurements of three different dry and wet stacks. (B) Area of the 3300 cm^{-1} band integrated over the range 3000−3700 cm^{-1} assigned to N−H stretching of polyamide[38] versus the number of layers, averaged over three independent measurements on different stacks.

detail elsewhere.[30,33] SWC4+ membrane was immersed in 1:1 water/ethanol solution, left for 10 min in an ultrasound bath, and afterward stored in DI water for 24 h. The water flux was stabilized for 8 h at 4 MPa. After stabilization, water permeability and rejection of organics solutes and corresponding permeate fluxes used in SFPF model were measured at pressure 2.1 MPa, temperature 298 K, and cross−flow velocity of 0.42 m s^{-1}. The ratio of permeate to feed flow was below 1%.

Six organic solutes were trimethylene oxide, 1,3-dioxolane, 1,4-dioxane, 12-crown-4, 15-crown-5, and 18-crown-6 (SI Table S2). Solutes were selected to be near-spherical and hydrophilic to minimize interaction with polyamide, and presumably nonsteric partitioning.[3] Note these criteria distinctly differed from those used for FTIR experiments; for this reason different solutes were used in the two sets of experiments. Mass transfer coefficients were estimated using the Sherwood correlation corresponding to feed spacer characteristics,[34] as described by Dražević et al.[33] Concentrations of organic solutes in permeate and retentate streams were determined using a Shimadzu TOC_{WS} Carbon Analyzer. The flux and solute rejections were fitted to the SFPF model to obtain the pore size distribution (PSD). The dominant pore radius in obtained PSD was taken as the effective pore radius, R_p.

Molecular Dynamics Simulation of Hydrated Polyamide. The molecular dynamics simulation used here is described in detail elsewhere.[22] Briefly, the polyamide structure was constructed through polymerization of diamine and triacid chloride monomers to closely match the experimentally obtained atomic composition of genuine fully cross-linked polyamide. The polymerization protocol employed the GAFF force field and GROMACS software package (ver. 4.6.3). Thus, the obtained polyamide structure was imported to molecular dynamics software to simulate the process of hydration and find the equilibrium state of the hydrated polyamide. Polyamide structure was equilibrated with water for 10 ns. Afterward, 100-ns long simulations of the hydrated polyamide were run and trajectories recorded and analyzed to plot the figures using the same parameters as described earlier.[22]

RESULTS AND DISCUSSION

RO Results: Estimates of Effective Pore Radius. Two estimates of the effective pore radius for SWC4+ membrane were obtained from RO experiments. One estimate of 0.23 nm was deduced from the hydraulic permeability and measured porosity using eq 6. It is in good agreement with recent positron annihilation lifetime study (PALS) measurements performed by Lee et al.[16] on a dense commercial SW30 membrane and similar homemade aromatic polyamide membranes (0.25 nm). The second estimate of effective pore size was obtained from rejection of several model solutes fitted to the SFPF model with a distribution of pore radii.[30,32] This yielded a sharp unimodal log-normal PSD with a dominant pore radius of 0.32 nm (SI Figure S2).[31] Even though some studies suggest that PSD in aromatic polyamide membranes may be bimodal,[35] the unimodal PSD was consistent with previous studies of dense RO membranes, such as SWC4+ used here.[17] The dominant pore radius 0.32 nm was used as the upper estimate of the effective pore radius. Given the sharp PSD with a standard deviation of about 0.02 nm, it was reasonable to replace it with a single effective radius. This radius was higher compared to 0.20−0.25 nm deduced from water permeation and PALS.[16,17] This could be partly explained by solute diffusion being ignored in SFPF model,[36] which however did not affect any conclusion below.

Thickness, Swelling, and Uniformity of the Stacks of Layers. The estimate of the diffusion coefficient in a film may be affected by its homogeneity. The selective layers in many polyamide composites, especially more open high-flux types, show significant depth heterogeneity. However, examination by transmission electron microscopy indicates that a single selective layer of SWC1, a seawater membrane analogous to SWC4+ used here, may be considered relatively homogeneous.[14,37]

Another potential source of inhomogeneity in the present case is the interlayer spaces between individual layers in the stack due to surface roughness and rigidity of individual layers. This effect was apparently minimized by the use of dimethylformamide as a solvent for PSU, which softened each PA layer in the entire stack each time a new layer was added. Given the identical chemistry of the layers, softened thin layers could then readily readjust and stick to the silicon wafer substrate and to each other by capillary and intermolecular forces forming a reasonably homogeneous planar stack.

Figure 2A shows the stack thickness measured by AFM versus the number of layers. The thickness was well reproducible and correlated in a highly linear manner with the number of layers, both for dry and wet films. AFM measurements were confirmed by ATR−FTIR measurements

dx.doi.org/10.1021/es502085p | Environ. Sci. Technol. XXXX, XXX, XXX−XXX

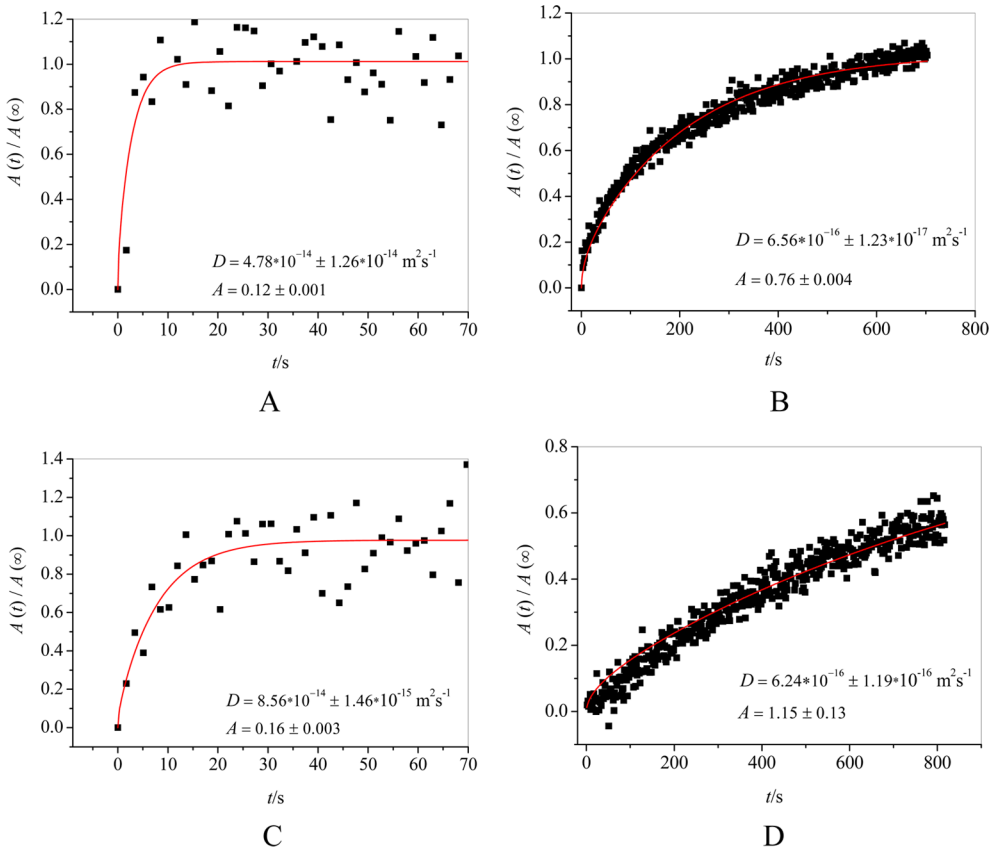

Figure 3. Typical measured variations of intensity $A(t)$ of the solute-specific bands (as band areas) vs time after solute injection for the hydrated stacks of 5 and 10 SWC4+ layers. Symbols represent experimental results scaled to the maximal value and lines represent two-parameter fits using eq 2. (A) 5-layer stack, ethylene glycol; (B) 5-layer stack, benzyl alcohol; (C) 10-layer stack, ethylene glycol, and (D) 10-layer stack, benzyl alcohol. For complete data see Supporting Information.

that also showed a good linear correlation of the N−H band area with the number of layers (Figure 2B). The thickness per one layer was also in good agreement with TEM observations.[14,37] These results suggest that the layers were densely packed and the whole stack was reasonably homogeneous.

ATR−FTIR Results: Effective Diffusivity of Organics. Figure 3 shows representative experimental data obtained from ATR−FTIR for 5- and 10-layer stacks along with corresponding fits to eq 2. The FTIR data obtained for faster diffusing solutes for 5-layer stacks are more scattered and noisier compared to slower diffusing solutes since the spectrum acquisition time, 1.64 s per spectrum, was commensurate with diffusion time. However, the error was reduced and reproducibility was improved by using a stack of 10 layers which allowed 4 times longer diffusion times, as seen in Figure 3.

The use of stacked layers also reduced the background signal due to evanscent wave reaching the bulk solution (compare SI Figures S3E and S4). Such a background was negligible in the measurements by Barbari and Fieldson,[26] where films thickness was much above the IR penetration depth $1/\gamma$. In the present case $1/\gamma \sim 2.5$ μm for the hydrated aromatic polyamide ($n_e \approx 1.60$), while the thickness d of the hydrated stacks of 5 and 10 layers was only about 1/4 and 1/2 of this value, respectively. If the solute concentration in the film were similar to solution, this could result in a background error of the order $e^{-2\gamma d}$ (cf. eq 1), i.e., a few tens percent. However, the background intensity for the same solution measured without a film plateaued immediately (SI Figure S4) after injection (i.e., within acquisition time of the first spectrum) at values much smaller than that with a film. Apparently, preferential partitioning in the film amplified the solute bands relative to the background (compare A values in SI Figures S3E and S4). Furthermore, the fitted diffusivity could be fairly robustly determined in most experiments regardless of the background intensity, since it must be of the order d^2/τ, where τ is the time required to reach the equilibrium plateau (see Figure 3) that was weakly affected by the background. Overall, the error in the fitted value of D was insignificant, given far larger deviations from HTT predictions, as discussed in the next section.

Comparison of ATR−FTIR Results with HTT. The Stokes radii of solutes used in diffusion experiments were in the range 0.2−0.27 nm. For this reason the lower estimate of the effective pore radius 0.23 nm could be meaningfully compared to HTT predictions only for the smallest ethylene glycol and glycerol, for which $\varphi < 1$. As shown in Figure 4, even for smaller pore radius, $R_p = 0.23$ nm, the diffusivity predicted (solid black line) for ethylene glycol ($R_s = 0.198$ nm) and glycerol ($R_s = 0.217$ nm) overestimates the measured diffusivity by 2 orders of magnitude. Obviously, the effective pore radius 0.23 nm does not represent consistently the pore space through which diffusion transport of the solute occurs. Figure 4 also compares measured diffusivities and HTT prediction for the upper estimate $R_p = 0.32$ nm. For this radius, HTT overestimates the diffusivity by almost 3 orders of magnitude (solid red line). The agreement with HTT predictions is then even poorer than for $R_p = 0.23$ nm. In either case, it is seen that, having adopted HTT as a framework for analyzing transport in the RO

dx.doi.org/10.1021/es502085p | Environ. Sci. Technol. XXXX, XXX, XXX−XXX

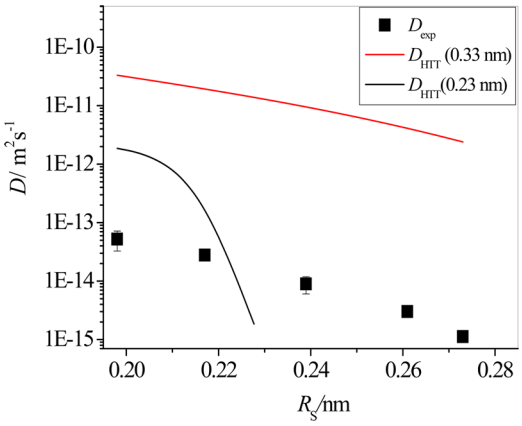

Figure 4. Measured diffusivities (symbols) and HTT estimates using eq 4 versus Stokes radii for lower (R_p = 0.23 nm, lower solid line) and upper bond (R_p = 0.32 nm, upper solid line) of pore radius.

membrane, which includes pore size and diffusivity calculations, a contradiction between experiment and theory is obtained. Following the classical *reductio ad absurdum* principle, it is concluded that HTT appears inadequate for calculating hindrance of molecular solutes within the polyamide.

This negative conclusion, however, does not reveal the reason for the failure. A plausible explanation might be that HTT in its simple form allows interaction with the pore walls only through viscous forces and exhibit a sharp size cutoff behavior. This ignores the possibility that other mechanisms of hindrance may operate. For instance, within molecular pores larger than R_s, enhanced molecular interactions with the polyamide matrix (e.g., via hydrogen bonds) may slow the diffusion more than bulk-like hydrodynamics predicts. On the other hand, pores smaller than R_s or even dense regions might be "soft" or elastic and thus pass the solute via thermally activated processes, e.g., transient pore widening or formation of a transient cavity in a dense polymer. Such activated processes have been considered in free-volume theories of solute diffusion in dense polymers and gels.[39−44] The corresponding energy barrier rapidly increases with solute size and should modify the size dependence beyond the purely hydrodynamic hindrance assumed in HTT. Indeed, it may be noticed in Figure 4 that the differences between the measured and the diffusivities predicted for pore radius 0.32 nm exponentially increase for larger solutes.

Given the above discrepancies, it is surprising why HTT may describe rejections fairly well[1] (SI Table S2). The present results suggest that this might be fortuitous, as a result of compensation by large partitioning, which may be fairly large for some solutes.[1,4] For instance, partitioning of *n*-alcohols was shown to increase with the solute size,[45] which partly offsets the effect of size on hindrance or activated transport. This emphasizes the advantage of the direct test of hindrance relations using direct approaches such as the one used here.

Modeling the Pore Geometry: Parallel Pore Array vs Random Resistor Network. In addition to dependence of hindrance on solute size, the model of parallel cylindrical pores, straight or tortuous, may be subject to criticism as well. Molecular dynamics simulations of the polyamide structure in Figure 5A display a typical 2D slice of the membrane showing distribution of the polymer density.[22] As mentioned in the Introduction, in this structure water fills randomly connected nanovoids widely varying in size and shape, which bear little resemblance to an array of parallel pores. This suggests that a more adequate description of such a system may be a random network of resistances. Larger water-filled voids may be viewed as "nodes" of the network. The "nodes" are connected by narrow passages or regions of low polymer density forming "bonds", widely varying in resistance. A useful concept for describing resistance of such networks is that of *a critical bond*. The latter is defined as the one that, along with all less resistant bonds, just forms a *percolating subnetwork*, for which the critical bond is essentially the bottleneck. The critical bond then marks the bond percolation threshold of the network. Figure 5B illustrates the idea: the nodes are shown as dots and the bonds of the percolating subnetwork are designated by solid lines. Thicker solid lines correspond to less resistant (subcritical) bonds, while the other, more resistant (supercritical) bonds are shown as dashed lines. The critical bond, just making the bond network connected, is the thinnest solid line. (Note that bonds and nodes are arranged in three dimensions thereby two-dimensional representation is merely an illustration.)

It was argued that for a wide distribution of resistances the macroscopic resistance of the whole network will be determined by *the resistance of the critical bond*.[46−48] Indeed, the subcritical bonds of the percolating subnetwork add little to

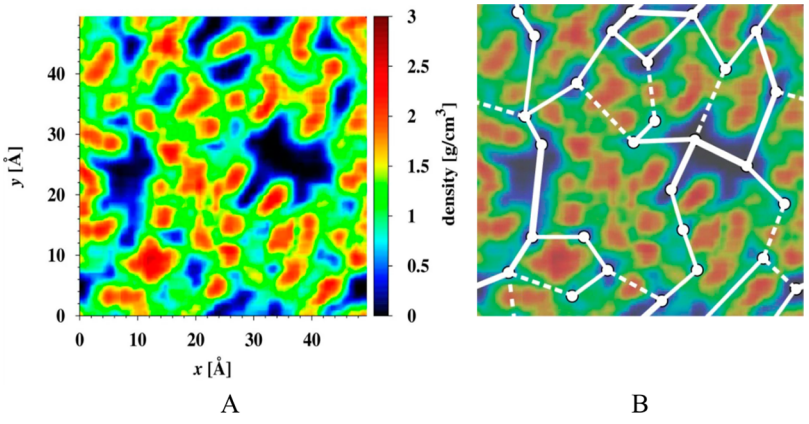

Figure 5. (A) Distribution of polyamide density within 50 × 50 Å^2 slice. (B) Illustration of the concept of "nodes" (shown as white dots) connected by "bonds" (lines). The solid lines represent subcritical bonds, while dashed lines represent supercritical bonds. The thinnest solid lines correspond to the critical bonds.

dx.doi.org/10.1021/es502085p | *Environ. Sci. Technol.* XXXX, XXX, XXX−XXX

the bottleneck resistance, while the supercritical bonds bypassing the critical bonds (dashed lines in Figure 5B) are too resistant to affect the overall resistance significantly.

When the resistor network replaces the parallel pore picture, the pore size of the critical bond will replace the effective pore size of the parallel pore arrays. This replacement will not be merely a formality, since there are two important distinctions between the two models. First, for a parallel array with a distribution of pores sizes, the effective pore size is a certain *weighed average* and thus it becomes obscured and dependent on the specific transport mechanism. In contrast, in a random network the critical pore size is determined by ranking of the pores by resistance and is thus much better defined and less mechanism-dependent. Second, the length of the pores in the parallel array geometry is identified with the films thickness, possibly corrected for tortuosity, whereas in a resistor network, the total length of critical pores is only a fraction of the film thickness. Making the pore length equal to the film thickness should then overestimate the critical pore size for a given permeability, which might be another reason for inconsistent pore size estimates by different methods.

In conclusion, the present results indicate that HTT does not adequately describe RO, NF, and similar molecular separation processes. To better reflect the structure and transport mechanism in RO and NF membranes, improved models may need to (a) replace rigid pores with a sharp cutoff, usually assumed in HTT, with elastic or transient pores, e.g., using the free-volume or similar activated transport theories, (b) replace the picture of a parallel pore array with that of a random resistor network, and (c) properly address solute partitioning.

Building an improved transport models along these lines, which was beyond the scope of this study, will be the subject of future work.

■ ASSOCIATED CONTENT

Supporting Information

Procedure for analysis of the effective pore size using SFPF model and results of ATR-FTIR and fits for all solutes. This material is available free of charge via the Internet at http://pubs.acs.org.

■ AUTHOR INFORMATION

Corresponding Author

*E-mail: vfreger@tx.technion.ac.il.

Notes

The authors declare no competing financial interest.

■ ACKNOWLEDGMENTS

E.D. and K.K. acknowledge the support by Croatian Science Foundation through project "Measuring of partitioning of organic solutes between polysulphone/polyamide films and water" and by the University of Zagreb through project "Removal of organic contaminants from water using advanced membrane processes of reverse osmosis and nanofiltration". V.F. and V.K. acknowledge the financial support by Israel Science Foundation through grant 1152/11.

■ REFERENCES

(1) Verliefde, A. R. D.; Cornelissen, E. R.; Heiman, S. G. J.; Hoek, E. M. V.; Amy, G. L.; Bruggen, B. V. D.; Dijk, J. C. V. Influence of solute-membrane affinity on rejection of uncharged organic solutes by nanofiltration membranes. *Environ. Sci. Technol.* **2009**, *43*, 2400−2406.

(2) Soltanieh, M.; Gill, W. Review of reverse osmosis membranes and transport models. *Chem. Eng. Commun.* **1981**, *12*, 279−363.

(3) Bellona, C.; Drewes, J. E.; Xu, P.; Amy, G. Factors affecting the rejection of organic solutes during NF/RO treatment—A literature review. *Water Res.* **2004**, *38*, 2795−2809.

(4) Dražević, E.; Bason, S.; Košutić, K.; Freger, V. Enhanced partitioning and transport of phenolic micropollutants within polyamide composite membranes. *Environ. Sci. Technol.* **2012**, *46* (6), 3377.

(5) Ferry, J. D. Statistical evaluation of sieve constants in ultrafilitration. *J. Gen. Physiol.* **1936**, *20*, 95−104.

(6) Brenner, H.; Gaydos, L. J. The constrained Brownian movement of spherical particles in cylindrical pores of comparable radius. *Colloid Interface Sci.* **1977**, *58*, 312−356.

(7) Bungay, P. M.; Brenner, H. The motion of a closely fitting sphere in a fluid-filled tube. *Int. J. Multiphase. Flow* **1973**, *1*, 25−56.

(8) Mavrovouniotis, G. M.; Brenner, H. Hindered sedimentation and dispersion coefficients for rigid, closely fitting Brownian spheres in circular cylindrical pores containing quiescent fluids. In *AIChE Annual Meeting, Miami Beach, Fl., November 2-7, 1986*; American Institute of Chemical Engineers: New York, 1986; Paper 85b.

(9) Deen, J. W. Hindered transport of large molecules in liquid-filled pores. *AIChE J.* **1987**, *33* (9), 1409−1425.

(10) Matsuura, T. *Synthetic Membranes and Membrane Separation Processes*; CRC Press, Taylor & Francis Group: Boca Raton, FL, 1993.

(11) Van der Bruggen, B..; Braeken, L.; Vandecasteele, C. Evaluation of parameters describing flux decline in nanofiltration of aqueous solutions containing organic compounds. *Desalination* **2002**, *147*, 281−288.

(12) Bowen, W. R.; Mohammad, A. W.; Hilal, N. Characterisation of nanofiltration membranes for predictive purposes - Use of salts, uncharged solutes and atomic force microscopy. *J. Membr. Sci.* **1997**, *126*, 91−105.

(13) Freger, V. Nanoscale heterogeneity of polyamide membranes formed by interfacial polymerization. *Langmuir* **2003**, *19*, 4791−4797.

(14) Freger, V. Swelling and morphology of the skin layer of polyamide composite membranes. *Environ. Sci. Technol.* **2004**, *38*, 3168−3175.

(15) Coronell, O.; Mariñas, B. J.; Cahill, D. G. Depth heterogeneity of fully aromatic polyamide active layers in reverse osmosis and nanofiltration membranes. *Environ. Sci. Technol.* **2011**, *45* (10), 4513−4520.

(16) Lee, J.; Doherty, C. M.; Hill, A. J.; Kentish, S. E. Water vapor sorption and free volume in the aromatic polyamide layer of reverse osmosis membranes. *J. Membr. Sci.* **2013**, *425−426*, 217−226.

(17) Kim, S.-H.; Kwak, S.-Y.; Suzuki, T. Positron annihilation spectroscopic evidence to demonstrate the flux-enhancement mechanism in morphology-controlled thin-film-composite (TFC) membrane. *Environ. Sci. Technol.* **2005**, *39* (6), 1764−1770.

(18) Harder, E.; Walters, D. E.; Bodnar, Y. D.; Faibish, R. S.; Roux, B. Molecular dynamics study of a polymeric reverse osmosis membrane. *J. Phys. Chem. B* **2009**, *113* (30), 10177−10182.

(19) Luo, Y.; Harder, E.; Faibish, R. S.; Roux, B. Computer simulations of water flux and salt permeability of the reverse osmosis FT-30 aromatic polyamide membrane. *J. Membr. Sci.* **2011**, *384* (1), 1−9.

(20) Ding, M.; Szymczyk, A.; Goujon, F.; Soldera, A.; Ghoufi, A. Structure and dynamics of water confined in a polyamide reverse-osmosis membrane: A molecular-simulation study. *J. Membr. Sci.* **2014**, *458*, 236−244.

(21) Hughes, Z. E.; Gale, J. D. A computational investigation of the properties of a reverse osmosis membrane. *J. Mater. Chem.* **2010**, *20*, 7788−7799.

(22) Kolev, V.; Freger, V. Hydration, porosity and water dynamics in the polyamide layer of reverse osmosis membranes: A molecular dynamics study. *Polymer* **2014**, *55* (6), 1420−1426.

(23) Frommer, M. A.; Murday, J. S.; Messalem, R. M. Solubility and diffusivity of water and of salt in aromatic polyamide film. *Eur. Polym. J.* **1973**, *9*, 367−373.

(24) Bason, S.; Oren, Y.; Freger, V. Characterization of ion transport in thin films using electrochemical impedance spectroscopy: II: Examination of the polyamide layer of RO membranes. *J. Membr. Sci.* **2007**, *302* (1−2), 10−19.
(25) Fieldson, G. T.; Barbari, T. A. The use of FTi.r.-a.t.r. spectroscopy to characterize penetrant diffusion in polymers. *Polym. Int.* **1993**, *34* (6), 1146−1153.
(26) Fieldson, G. T.; Barbari, T. A. Analysis of diffusion in polymers using evanescent field spectroscopy. *AIChE J.* **1995**, *41* (4), 795−804.
(27) Bruggeman, D. A. G. Berechnung verschiedener physikalischer Konstanten von heterogenen Substanzen. I. Dielektrizitätskonstanten und Leitfähigkeiten der Mischkörper aus isotropen Substanzen. *Ann. Phys. (Berlin, Ger.)* **1935**, *416* (7), 636−664.
(28) Dražević, E.; Košutić, K.; Freger, V. Permeability and selectivity of reverse osmosis membranes - Correlation to swelling revisited. *Water Res.* **2014**, *49*, 444−452.
(29) Bason, S.; Kaufman, Y.; Freger, V. Analysis of ion transport in nanofiltration using phenomenological coefficients and structural characteristics. *J. Phys. Chem. B* **2010**, *114*, 3510−3517.
(30) Dražević, E.; Košutić, K.; Dananić, V.; Pavlović, D. M. Coating layer effect on performance of thin film nanofiltration membrane in removal of organic solutes. *Sep. Purif. Technol.* **2013**, *118*, 530−539.
(31) Torquato, S. *Random Heterogeneous Materials: Microstructure and Macroscopic Properties*; Springer: New York, 2002; Vol. *16*.
(32) Sourirajan, S.; Matsuura, T. *Reverse Osmosis/Ultrafiltration Process Principles*; National Research Council Canada: Ottawa, 1987; Ch. 4, pp 279−358.
(33) Dražević, E.; Košutić, K.; Dananić, V. Mass transfer of differently sized organic solutes at spacer covered and permeable nanofiltration wall. *Chem. Eng. J.* **2014**, *244*, 152−159.
(34) Koutsou, C. P.; Yiantsios, S. G.; Karabelas, A. J. A numerical and experimental study of mass transfer in spacer-filled channels: Effects of spacer geometrical characteristics and Schimdt number. *J. Membr. Sci.* **2009**, *326*, 234−251.
(35) Košutić, K.; Kaštelan-Kunst, L.; Kunst, B. Porosity of some commercial reverse osmosis and nanofiltration polyamide thin film composite membranes. *J. Membr. Sci.* **2000**, *168*, 101−108.
(36) Mehdizadeh, H.; Dickson, J. M. Theoretical modifications of the surface force-pore flow model for reverse osmosis transport. *J. Membr. Sci.* **1989**, *42*, 119−145.
(37) Pacheco, C. A.; Pinnau, I.; Reinhard, M.; Leckie, J. O. Characterization of isolated polyamide thin films of RO and NF membranes using novel TEM techniques. *J. Membr. Sci.* **2010**, *358*, 51−59.
(38) Skrovanek, D. J.; Howe, S. E.; Painter, P. C.; Coleman, M. M. Hydrogen bonding in polymers: Infrared temperature studies of an amorphous polyamide. *Macromolecules* **1985**, *18*, 1676−1683.
(39) Fujita, H., Diffusion in polymer-diluent systems. In *Fortschritte Der Hochpolymeren-Forschung*; Springer Berlin Heidelberg: Berlin, 1961; Vol. *3/1*.
(40) Vrentas, J. S.; Duda, J. L.; Ling, H.-C. Free-volume theories for self-diffusion in polymer−solvent systems. I. Conceptual differences in theories. *J. Polym. Sci. Polym. Phys. Ed.* **1985**, *23* (2), 275−288.
(41) Vrentas, J. S.; Vrentas, C. M. Predictive methods for self-diffusion and mutual diffusion coefficients in polymer−solvent systems. *Eur. Polym. J.* **1998**, *34*, 797−803.
(42) Peppas, N. A.; Reinhart, C. T. Solute diffusion in swollen membranes. Part I: A new theory. *J. Membr. Sci.* **1983**, *15*, 275−287.
(43) Cohen, M. H.; Turnbull, D. Molecular transport in liquids and glasses. *J. Chem. Phys.* **1959**, *31*, 1164−1169.
(44) Freeman, B. D. Basis of permeability/selectivity tradeoff relations in polymeric gas separation membranes. *Macromolecules* **1999**, *32* (2), 375−380.
(45) Ben-David, A.; Oren, Y.; Freger, V. Thermodynamic factors in partitioning and rejection of organic compounds by polyamide composite membranes. *Environ. Sci. Technol.* **2006**, *40* (22), 7023−7028.
(46) Ambegaokar, V.; Halperin, B. I.; Langer, J. S. Hopping conductivity in disordered systems. *Phys. Rev. B* **1971**, *4*, 2612−2620.
(47) Pollak, M. A percolation treatment of dc hopping conduction. *J. Non-Cryst. Solids* **1972**, *11*, 1−24.
(48) Feng, S.; Halperin, B. I.; Sen, P. N. Transport properties of continuum systems near the percolation threshold. *Phys. Rev. B* **1987**, *35*, 197−214.